Geophys. J. Int. (2009) **177,** 966–977 doi: 10.1111/j.1365-246X.2009.04147.x

FAST TRACK PAPER

Receiver function decomposition of OBC data: theory

Pascal Edme[1] and Satish C. Singh[2]

[1] *Schlumberger Cambridge Research (formerly at IPG Paris). E-mail: epascal@slb.com*
[2] *IPG Paris. E-mail: singh@ipgp.jussieu.fr*

Accepted 2009 February 12. Received 2009 February 12; in original form 2008 September 11

SUMMARY

This paper deals with theoretical aspects of wavefield decomposition of Ocean Bottom Cable (OBC) data in the $\tau-p$ domain, considering a horizontally layered medium. We present both the acoustic decomposition and elastic decomposition procedures in a simple and compatible way. Acoustic decomposition aims at estimating the primary upgoing *P* wavefield just above the ocean-bottom, whereas elastic decomposition aims at estimating the primary upgoing *P* and *S* wavefields just below the ocean-bottom. Specific issues due to the interference phenomena at the receiver level are considered. Our motivation is to introduce the two-step decomposition scheme called 'receiver function' (RF) decomposition that aims at determining the primary upgoing *P* and *S* wavefields (RF_P and RF_S, free of any water layer multiples). We show that elastic decomposition is a necessary step (acting as pre-conditioning) before applying the multiple removal step by predictive deconvolution. We show the applicability of our algorithm on a synthetic data example.

Key words: Controlled source seismology; Body waves; Theoretical seismology; Wave propagation.

GJI Seismology

1 INTRODUCTION

With multicomponent OBC experiment, three orthogonal components of particle velocity and pressure fields are recorded. This type of data enables one to analyse the recordings in a vector-oriented manner and requires a different kind of processing from the conventional vertical component data alone. The key element in the OBC data processing is the way the different components are combined. By taking into account the additional measurements of the horizontal geophone and hydrophone sensor along with the vertical geophone data in the processing flow, more reliable information about the subseafloor properties can be obtained. In OBC surveys, the source is generally a towed airgun array producing pressure wave only; however, OBC data are not pure *P* or *S* wave but a superposition of upgoing and downgoing *P* and *S* waves. Therefore it is important to decompose the recordings into pure wavefields, that is, upgoing *P* and *S* wavefields (if possible free of water layer related multiples), prior to analysing pre- or post-stack data (Schalkwijk *et al.* 2003). There are several methods for performing a wavefield decomposition of OBC data. Depending on the level of the decomposition (i.e. above or below the ocean-bottom, see Fig. 1), they can be divided into two main categories:

The acoustic decomposition is performed just above the ocean-bottom level and aims at estimating the acoustic upgoing and downgoing P-wavefields propagating in the water layer. This kind of decomposition involves the combination of the vertical geophone and hydrophone component data and is often referred to as the *PZ* summation or as the dual-sensor method. Some of the early methods for combining these components to attenuate energy arriving from above through the water column were developed by Haggerty (1956), White (1965), Gal'perin (1974) and Loewenthal *et al.* (1985). The dual sensor method was presented by Barr & Sanders (1989), and further extended by Dragoset & Barr (1994), Paffenholz & Barr (1995), Barr (1997) and Barr *et al.* (1997). The summation procedure was originally derived for normal incidence angles in the time–space domain. In the last few years, a number of refinements and variations on these methods have been presented by Ball & Corrigan (1996), Bale (1998), Soubaras (1996), Osen *et al.* (1999) and Liu *et al.* (1999). However, these methods suffer from the fact that there are many events at a constant offset that arrive at different angles, and hence the approximation breaks down. Recently, the acoustic decomposition procedure has been implemented in the $\tau-p$ domain (τ being the intercept time, p the horizontal slowness) and is therefore valid for all incidence angles (Lokshtanov 1993, 1995, 2000; Soudani *et al.* 2005, 2006).

The elastic decomposition is performed just below the ocean-bottom level and aims at determining the upgoing *P*- and *S*-wavefields at the receiver level. Some of the existing methods are based on polarization analysis (Cho & Spencer 1992; Wang *et al.* 2002) or on the elastic wave equation formalism, where wavefields are expressed in terms of stress and potential. Applications of these decomposition methods have been discussed in Amundsen & Reitan (1995), Donati & Stewart (1996), Holvik & Amundsen (1998), Amundsen *et al.* (1998), Soubaras (1998), Holvik *et al.*

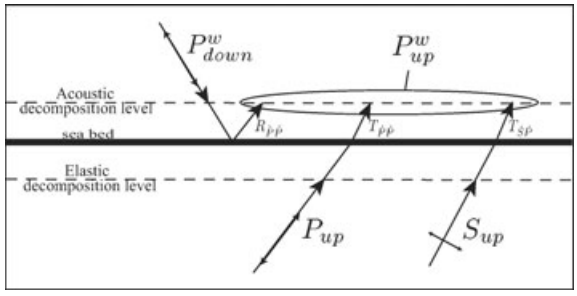

Figure 1. Decomposition level. The acoustic decomposition is performed just above the sea-bottom, whereas the elastic decomposition needs to be performed just below the sea-bottom. The $P_{\rm up}$, $S_{\rm up}$ and $P^w_{\rm down}$ are incident wavefields, whereas the $P^w_{\rm up}$ is a resulting wavefield, generated by reflection–transmission at the sea–bed interface.

(1999), Schalkwijk (2001), Amundsen *et al.* (2001), Schalkwijk *et al.* (2003), Muijs *et al.* (2004, 2007), as a modification of multicomponent decomposition schemes by White (1965), Dankbaar (1985) and Wapenaar *et al.* (1990). These methods require the knowledge of the elastic properties in the vicinity of the receiver and are usually applied in the ω–k domain (ω being the angular frequency, k the wave-number) or in the τ–p domain.

In this paper, we present both the acoustic and elastic decomposition procedures in a simple and compatible way. We restrict ourselves to the case of a horizontally layered medium. Theoretical aspects of OBC data decomposition are described in the τ–p domain, properly taking into account the seafloor interface effect and the systematic interference effects encountered in a marine environment. In a given p trace, many problems become less difficult because each incident wave arrives with a different but constant incident angle and the multiple's reverberation is periodic. Our goal is to introduce the fundamental equations required to apply what we call the Receiver Function (RF) decomposition, that is, upgoing *P*-S separation followed by predictive deconvolution to recover the pure primary RF_P and RF_S wavefields (free of any water layer multiples).

2 OBC DATA SPECIFICATIONS

With OBC data, it is assumed that the geophone sensors are located just below the seafloor (in the solid medium), whereas the hydrophone sensor is located just above the seafloor (in the liquid medium). All these recorded components result from the interaction of three types of incoming wavefields (upgoing *P*, upgoing *S*, downgoing *P*) with the seafloor interface in the vicinity of the sensors:

$$\begin{aligned} U_h &= U_h^{\grave{P}} + U_h^{\acute{P}} + U_h^{\acute{S}}, \\ U_z &= U_z^{\grave{P}} + U_z^{\acute{P}} + U_z^{\acute{S}}, \\ U_x &= U_x^{\grave{P}} + U_x^{\acute{P}} + U_x^{\acute{S}}, \end{aligned} \tag{1}$$

where U_x, U_z are the vertical and in-line horizontal geophone data and U_h is the pressure wavefield recorded by the hydrophone sensor. Since we are discussing wavefields in the vertical plane containing the OBC, we do not consider the U_y component here, but the theory could be easily extended. In the above equation, $U_i^{\grave{P}}$ denotes the recorded wavefield on the i component ($i = x, z, h$) considering an incident downgoing $\grave{P}$ wave (necessarily arriving from above at the receiver level), whereas $U_i^{\acute{P}}$ and $U_i^{\acute{S}}$ denote the recorded wavefields on the i component considering, respectively, an incident upgoing $\acute{P}$ wave and an upgoing $\acute{S}$ wave (necessarily arriving from below at the receiver level). In other words, the superscript ($\acute{P}$, $\acute{S}$ or $\grave{P}$) merely denotes the incident wave type, or equivalently the parent wave type, that will generate both upgoing and downgoing *P* and *S* motion when interacting with the seafloor interface (as discussed later in Section 2.1). Note therefore that U_i^j is not the contribution of the j wavefield on the i component, because in this latter case, we would have to consider a downgoing *S* wavefield as well. In contrast, using our notation (i.e. superscript = parent wave type), the *S* wavefield cannot be downgoing (arriving from above the seafloor) because the water does not support *S* wave propagation. As a consequence, because the hydrophone is located in the water, $U_h^{\acute{S}}$ is not the *S* wavefield recorded at the hydrophone level but the *S*-to-*P* wavefield converted at the ocean-bottom. Finally, note that these incident waves often arrive simultaneously (as described later in Section 2.2) and that the partitioning of the energy between the components depends on the seafloor interface properties.

2.1 Seafloor interface effect

As shown in eq. (1), the recorded wavefields are combination of up- and downgoing *P* and *S* waves arriving at the seafloor. Therefore, the seafloor interface effects should be taken into account during the wavefield decomposition. Here, we extend the method of Wang *et al.* (2002), by including the hydrophone measurement in addition to the geophone recordings. This is necessary to separate the three incident wavefields. In contrast to other existing methods that consist of estimating all propagating wavefields in the vicinity of the receivers, our approach consists of estimating only the incident wavefields ($P_{\rm up}$, $S_{\rm up}$ and $P^{\rm w}_{\rm down}$). As shown in Fig. 1, $P_{\rm up}$ and $S_{\rm up}$ are the pure elastic *P* and *S* wavefields, arriving as upgoing events just below the seafloor interface, whereas $P^{\rm w}_{\rm down}$ is the acoustic downgoing *P* wavefield in the water just above the seafloor. The recordings are composed of the superposition of the incident wavefields with their reflection–transmission conversion at the solid–liquid interface. In the τ–p domain, the three recorded components can be written as a linear combination of the three incident wavefields in a matrix form:

$$\begin{bmatrix} U_z \\ U_x \\ U_h \end{bmatrix} = \begin{bmatrix} M_{11} & M_{12} & M_{13} \\ M_{21} & M_{22} & M_{23} \\ M_{31} & M_{32} & M_{33} \end{bmatrix} \begin{bmatrix} P_{\rm up} \\ S_{\rm up} \\ P^{\rm w}_{\rm down} \end{bmatrix}, \tag{2}$$

where M is a matrix that depends on the ray parameter (or horizontal slowness) p and elastic properties near the receiver. It is interesting to note that even though the geophones are physically located in the solid media, just below the interface, the vertical geophone sensor U_z can be assumed to be located in the water layer (as the hydrophone) because of the continuity of the vertical displacement across a solid–liquid interface (Kennett 1983; Chapman 2004). This simplifies the expressions for the M_{1j} coefficients. Furthermore, the hydrophone is not sensitive to the direction of propagation of waves (in contrast to the geophones) and records the pressure as opposed to the particle velocities recorded by the geophones. Therefore, the hydrophone measurement needs to be divided by the acoustic impedance of the water to make the amplitudes of the hydrophone and geophones comparable [$U_h = P/(\rho_{\rm w}\alpha_{\rm w})$, where P is the pressure wavefield, $\rho_{\rm w} = 1\,{\rm g\,cm^{-3}}$ and $\alpha_{\rm w} = 1.5\,{\rm km\,s^{-1}}$ are the density and *P* wave velocity in water]. This can be viewed as a theoretical calibration step to compensate for the fact that the two types of recording do not have the same units. In practice, with real data, note that the calibration procedure is a crucial step (commonly requiring the use of frequency-dependent

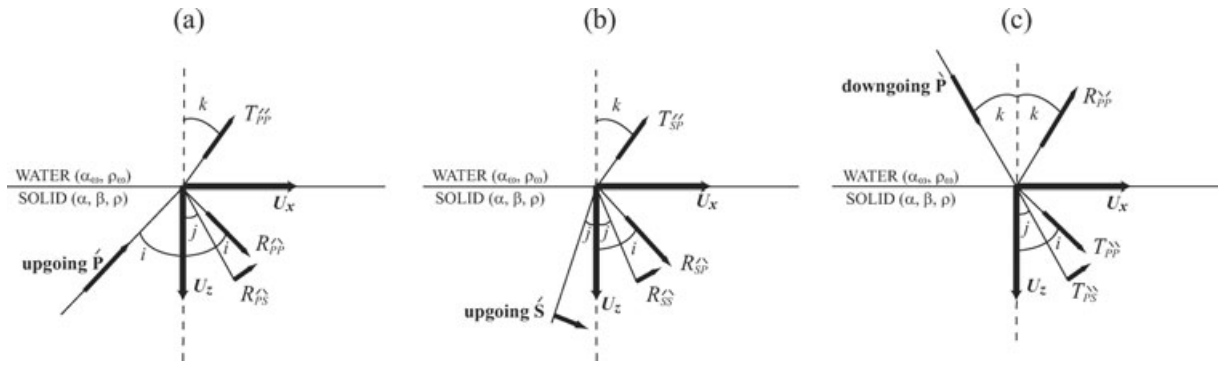

Figure 2. Seafloor interface effect, that is, reflection–transmission at the liquid-solid interface in the vicinity of the receiver. (a) For an upgoing P wave, giving the M_{i1} coefficients. (b) For an upgoing S wave, giving the M_{i2} coefficients. (c) For a downgoing P wave, giving the M_{i3} coefficients. i and j are the P and S wave propagation angles in the solid medium. k is the P wave propagation angle in the water. i, j and k are linked with the horizontal slowness by: $p = \frac{\sin i}{\alpha} = \frac{\sin k}{\alpha_w} = \frac{\sin j}{\beta}$.

operator rather than a scalar coefficient) that aims to compensate also for the fact that the two types of sensors have different impulse responses and different coupling with the ground. A powerful approach to achieve the calibration, automatically and directly from the data themselves, has been proposed by Soubaras (1996), based on the cross-ghosting process.

Let us consider an upgoing P wave as shown in Fig. 2(a), the recorded wavefields depend on the M_{i1} coefficients:

$$U_z^{\dot{P}} = M_{11} P_{\rm up} = (-q_{\rm w}\alpha_{\rm w} T_{\dot{P}\dot{P}}) P_{\rm up}, \tag{3}$$

$$U_x^{\dot{P}} = M_{21} P_{\rm up} = (p\alpha + R_{\dot{P}\dot{P}} p\alpha + R_{\dot{P}\grave{S}} q_\beta \beta) P_{\rm up}, \tag{4}$$

$$U_h^{\dot{P}} = M_{31} P_{\rm up} = (T_{\dot{P}\dot{P}}) P_{\rm up}. \tag{5}$$

Let us consider an upgoing S wave as shown in Fig. 2(b), the recorded wavefields depend on the M_{i2} coefficients:

$$U_z^{S} = M_{12} S_{\rm up} = (-q_{\rm w}\alpha_{\rm w} T_{\dot{S}\dot{P}}) S_{\rm up}, \tag{6}$$

$$U_x^{S} = M_{22} S_{\rm up} = (q_\beta \beta + R_{\dot{S}\grave{S}} q_\beta \beta + R_{\dot{S}\dot{P}} p\alpha) S_{\rm up}, \tag{7}$$

$$U_h^{S} = M_{32} S_{\rm up} = (T_{\dot{S}\dot{P}}) S_{\rm up}. \tag{8}$$

Let us consider an downgoing P wave as shown in Fig. 2(c), the recorded wavefields depend on the M_{i3} coefficients:

$$U_z^{\grave{P}} = M_{13} P^{\rm w}_{\rm down} = -q_w \alpha_w (1 - R_{\dot{P}\dot{P}}) P^{\rm w}_{\rm down}, \tag{9}$$

$$U_x^{\grave{P}} = M_{23} P^{\rm w}_{\rm down} = (T_{\dot{P}\dot{P}} p\alpha - T_{\dot{P}\grave{S}} q_\beta \beta) P^{\rm w}_{\rm down}, \tag{10}$$

$$U_h^{\grave{P}} = M_{33} P^{\rm w}_{\rm down} = (1 + R_{\dot{P}\dot{P}}) P^{\rm w}_{\rm down}, \tag{11}$$

where α, β and ρ are the P wave velocity, the S wave velocity and the density values just below the seafloor, in the vicinity of the geophones. The vertical slownesses for P and S waves are $q_\alpha = \sqrt{\alpha^{-2} - p^2}$ and $q_\beta = \sqrt{\beta^{-2} - p^2}$, respectively. The expressions for the reflection–transmission coefficients at the solid–liquid interface can be derived from the Zoeppritz equation (Wang *et al.* 2002)

$$\begin{aligned}
R_{\dot{P}\dot{P}} &= \left[-(1-2p^2\beta^2)^2 \rho q_{\rm w} + 4p^2\beta^4 \rho q_\alpha q_{\beta_1} q_{\rm w} + \rho_{\rm w} q_\alpha\right]/D,\\
T_{\dot{P}\dot{P}} &= 2\alpha\alpha_{\rm w}^{-1} \rho q_\alpha (1-2p^2\beta^2)/D,\\
R_{\dot{P}\grave{S}} &= 4\alpha\beta p \rho q_\alpha q_{\rm w} (1-2p^2\beta^2)/D,\\
R_{\grave{S}\grave{S}} &= \left[(1-2p^2\beta^2)^2 \rho q_{\rm w} - 4p^2\beta^4 \rho_1 q_\alpha q_\beta q_{\rm w} + \rho_{\rm w} q_\alpha\right]/D,\\
R_{\grave{S}\dot{P}} &= 4\alpha^{-1}\beta^3 p \rho q_\beta q_{\rm w} (1-2p^2\beta^2)/D,\\
T_{\grave{S}\dot{P}} &= -4\alpha_{\rm w}^{-1}\beta^3 p \rho q_\alpha q_\beta / D,\\
R_{\dot{P}\dot{P}} &= \left[(1-2p^2\beta^2)^2 \rho_1 q_{\rm w} + 4p^2\beta^4 \rho q_\alpha q_{\beta_1} q_{\rm w} - \rho_{\rm w} q_\alpha\right]/D,\\
T_{\dot{P}\dot{P}} &= 2\alpha_{\rm w}\alpha^{-1}(1-2p^2\beta^2)\rho_{\rm w} q_{\rm w}/D,\\
T_{\dot{P}\grave{S}} &= -4\alpha_{\rm w}\beta p \rho_{\rm w} q_\alpha q_{\rm w}/D,\\
D &= (1-2p^2\beta^2)^2 \rho q_{\rm w} + 4p^2\beta^4 \rho q_\alpha q_\beta q_{\rm w} + \rho_{\rm w} q_\alpha.
\end{aligned}$$

The eqs (2)–(11) describe the seafloor interface effect on the recorded data. Note that the inversion of the matrix M (eq. 2) will enable us to recover the incident wavefields of interest ($P_{\rm up}$, $S_{\rm up}$ and $P^{w}_{\rm down}$) from the recorded components (see Section 3).

2.2 Overlapping problems

In OBC data, when horizontally layered media are assumed, two important overlapping phenomena have to be considered. First, the P-to-S reflected waves ($\dot{P}\dot{P}\dot{S}$) arrive at the same time as the S-to-P reflected waves ($\dot{P}\grave{S}\dot{P}$). Therefore, except for the $\dot{P}\grave{S}\grave{S}$ waves (i.e. rays propagating exclusively as S wave in the subseafloor), 'pure' upgoing S waves do not exist in OBC data. Second, the pegleg arrivals (source-side multiples, upgoing at the receiver level) and the ghost arrivals (receiver-side multiples, downgoing at the receiver level) always arrive simultaneously. Therefore, 'pure' multiples do not exist in the data (except for those corresponding to the effective source function $Src_{\rm eff}$, that is, the direct arrival and its associated multiples confined in the water layer). On the U_h component, because the hydrophone sensor is insensitive to the direction of propagation of waves, the combination of upgoing and downgoing P multiples leads to a constructive summation. In contrast, since the geophones are sensitive to the direction of propagation, the superposition of multiples on the U_z component yields to a destructive summation. Therefore, the multiples are enhanced on the hydrophone component and are reduced on the vertical component.

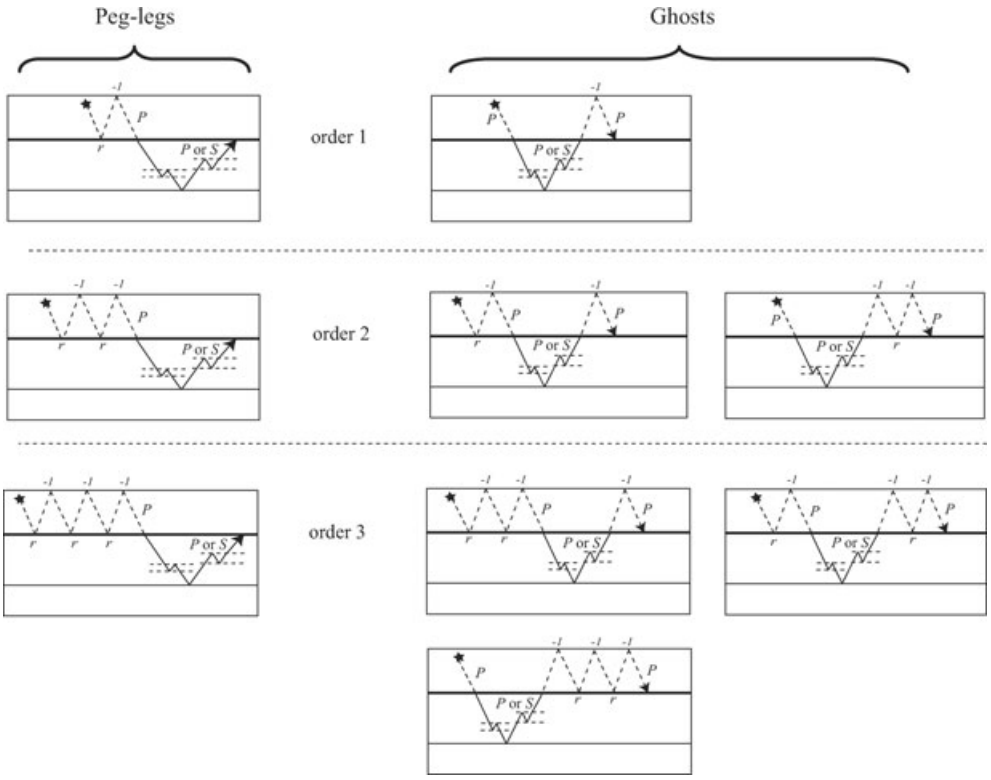

Figure 3. Left-hand panel: Family of ray paths for the peg-leg arrivals. The reverberation pattern is of the form $(1 + rZ_w)^{-1}$. The decay of amplitude is linear as a function of the multiple's order. Right-hand panel: Family of ray paths for the ghost arrivals. The reverberation pattern is of the form $(1 + rZ_w)^{-2}$. The decay of energy is not linear as a function of the multiple's order.

The effect of the superposition between the ghosts and the peg-legs is quite complex because it depends on the number of times the multiple has travelled in the water layer (i.e. the multiple order). Let us first consider a pure peg-leg event (as shown in Fig. 3 left-hand panel) that reverberates in the water layer before it propagates in the subseafloor. The reverberation pattern of peg-legs has a linear form described by:

$$1 - rZ_{\mathrm{w}} + r^2 Z_{\mathrm{w}}^2 - r^3 Z_{\mathrm{w}}^3 \ldots \approx (1 + rZ_{\mathrm{w}})^{-1}, \tag{12}$$

where $r = R_{\dot{P}\dot{P}}$ is the P wave reflection coefficient at the ocean-bottom and $Z_{\mathrm{w}}(\omega, p) = \mathrm{e}^{-2i\omega z_{\mathrm{w}} q_{\mathrm{w}}}$ is the two way traveltime operator of the water layer in the frequency domain (ω is angular frequency and z_w the water depth). Such a reverberation pattern is fully predictable, both in terms of arrival time (z_w is constant) and of amplitude (the amplitude of the multiples decays linearly as a function of the multiple order, or equivalently the amplitude ratio between order n and $n + 1$ is always $-r$). Therefore, pure peg-legs (free of overlapping problems with other wave types) can be easily removed by convolution with a linear filter of the form $1 + rZ_w$, which can be derived using the predictive deconvolution procedure (see Robinson 1957; Treitel 1974; Lines & Treitel 1984; Yilmaz 1987). The above statement is true for any possible ray path (including intrabed multiple reverberations, as illustrated in Fig. 3), except for the case of the rays that experience one (or more) downward reflection at the seafloor before being recorded, as shown in Fig. 4. In this latter case, the ratio between the parent event (order 0) and its water multiple (order 1) will differ from $-r$ because of the additional contribution of the ray, whose water layer reverberation is not at the onset of the propagation path (but still arrives at the receiver as an upgoing event, as shown in the bottom right-hand sketch of Fig. 4). Such multiples will only be attenuated by the predictive deconvolution, not fully removed. However, note that these events are free-surface related multiples of seabed-surface related multiples, which already have weak amplitudes compared with the primaries of interest. To a first-order approximation, these events can be neglected.

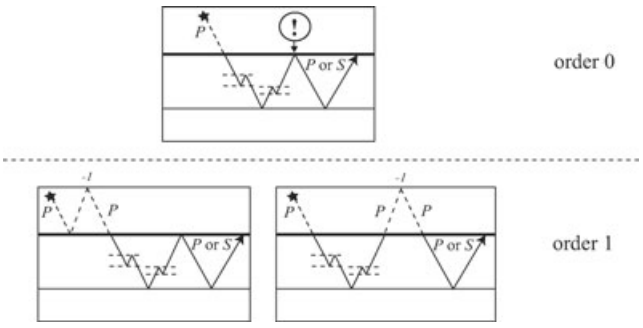

Figure 4. Example of upgoing event, whose reverberation pattern differs from that of peg-legs shown in Fig. 3 left-hand panel. The multiples will not be perfectly removed by predictive deconvolution. However, the order 0 has already weak amplitude compared with primaries and, to a first-order approximation, the residual multiples can be neglected.

Now let us consider the ghost arrivals (Fig. 3 right-hand panel), that is, the multiples arriving from above as downgoing P waves at the receiver, just after at least one water column reverberation. Such multiples may include some source-side water reverberations as well. By taking into account both source and receiver sides of multiple paths, the reverberation pattern of ghost arrivals can be written as:

$$1 - 2rZ_w + 3r^2 Z_w^2 - 4r^3 Z_w^3 \ldots \approx (1 + rZ_w)^{-2}. \tag{13}$$

This reverberation pattern is predictable in time (once again Z_w is constant), but the amplitude decay of multiple varies as a function of the multiple order (in contrast to the peg-leg case, eq. 12). For example, the amplitude decay between the first and the second multiple is equal to $-2r$, whereas the amplitude decay between the second and the third multiple is equal to $-\frac{3}{2}r$.

The above two equations clearly show that overlapping of peg-legs and ghosts have to be taken into account, in the presence of a water layer. For instance, Fig. 3 shows that one ghost interferes with one peg-leg if we consider the first-order multiples, whereas two ghosts overlap with only one peg-leg if we consider the second multiples order. This demonstrates that a conventional predictive deconvolution is only suitable to remove pure peg-leg events but is not suitable to remove overlapping ghosts and peg-legs. This problem makes the multiple removal stage more complex if upgoing and downgoing wavefields are not previously well separated.

3 RF DECOMPOSITION EQUATIONS

As already mentioned, the inversion of the matrix **M** (eq. 2) enables us to recover the incident wavefields $P_{\rm up}$, $S_{\rm up}$ and $P^{\rm w}_{\rm down}$ from the recorded components (U_z, U_x, U_h) in the τ–p domain. Further, the outgoing $P^{\rm w}_{\rm up}$ can be expressed as a function of these incident wavefields as illustrated in Fig. 1:

$$P^{\rm w}_{\rm up} = R_{\grave{P}\acute{P}} P_{\rm down} + T_{\grave{P}\acute{P}} P_{\rm up} + T_{\grave{S}\acute{P}} S_{\rm up}. \tag{14}$$

We can now describe two different RF decomposition schemes, referred to as elastic and acoustic (depending on the level of the decomposition as described in Fig. 1) and illustrated in Figs 5 and 6, respectively. We start with the original (recorded) traces in the τ–p domain, taking into account the seafloor interface effect as well as the reverberation patterns of the water multiples. In these sketches, the primaries are shown by solid lines, whereas the multiples are shown in dashed lines. The first arrival is the first break, the following primary event is the reflected $\grave{P}\grave{P}\acute{P}$ wave, then arrive the $\grave{P}\grave{P}\acute{S}$ and $\grave{P}\grave{S}\acute{P}$ waves at the same time and, finally, is the $\grave{P}\grave{S}\acute{S}$ event that propagates exclusively as S wave in the subseafloor. Note that on the hydrophone component data U_h, the amplitude of the first-order multiple (relative to a given primary arrival) is given by $1 + 2r$; so, it is always bigger than the primary arrival (the reflection coefficient $r = R_{\grave{P}\acute{P}}$ is always positive). In contrast, the first-order multiple amplitude (relative to a given primary arrival) is equal to $1 - 2r$ on the U_z component. As a consequence, when $r = 0.5$, the first-order multiples are fully attenuated on U_z, whereas they are twice as big as the primaries on the U_h component. On the horizontal U_x component, the behaviour is more complex.

3.1 Elastic case

The elastic decomposition aims at determining the upgoing P and S wavefields, propagating in the solid medium just below the ocean-bottom. The expressions for the $P_{\rm up}$ and $S_{\rm up}$ wavefields are obtained by inverting eq. 2 and involve the three recorded components:

$$P_{\rm up} = U_z - \frac{q_\alpha}{1 - 2p^2\beta^2}\left(2p\beta^2 U_x + \frac{\alpha_{\rm w}\rho_{\rm w}}{\rho} U_h\right), \tag{15}$$

$$S_{\rm up} = U_x - \frac{p}{(1 - 2p^2\beta^2)}\left(\frac{\alpha_{\rm w}\rho_{\rm w}}{\rho} U_h - 2q_\beta\beta^2 U_z\right). \tag{16}$$

Note that here we chose to normalize these equations such that (1) the coefficient before U_z is one for the $P_{\rm up}$ expression and (2) the coefficient before U_x is one for the $S_{\rm up}$ expression. This means that we assume that U_z contains predominately upgoing P waves and U_x contains predominately upgoing S waves. By applying these equations (first step in Fig. 5), we extract the P and S events arriving as upgoing wave at the receiver level, and therefore we partially address the problem of multiples in the data by removing all the ghost arrivals. However, note that this does not mean that the amount of multiples is weaker on the decomposed upgoing $P_{\rm up}$ and $S_{\rm up}$ wavefields than on the original U_z and U_x components. This depends on the P-wave reflection coefficient value at the ocean-bottom (see Fig. 5). In a given p trace, $P_{\rm up}$ contains less first-order multiple energy than U_z only if $r < 0.33$ (i.e. $r < 1 - 2r$).

Then the remaining multiples (pure peg-leg arrivals) can be eliminated from the previously separated $P_{\rm up}$ and $S_{\rm up}$ wavefields by applying a single time-shifted subtraction for each p trace:

$$RF_P = P_{\rm up}(1 + r Z_w), \tag{17}$$

$$RF_S = S_{\rm up}(1 + r Z_w), \tag{18}$$

which is equivalent to applying predictive deconvolution (i.e. time-shifted adaptive subtraction) when r is unknown.

This second step, giving the RF_P and RF_S traces that contain only primary events arriving as P and S waves (respectively) at the receiver level, is also schematically illustrated in Fig. 5. This simple approach is efficient because the reverberation pattern of peg-legs in $P_{\rm up}$ and $S_{\rm up}$ is fully predictable, that is, $(1 + r Z)^{-1}$ (eq. 12). In other words, the first step acts as a pre-conditioning step to allow water multiple removal, using predictive deconvolution.

3.2 Acoustic case

The acoustic decomposition aims at separating the downgoing and upgoing P wave, propagating in the water just above the ocean-bottom. The expression for the $P^{w}_{\rm down}$ wavefield results from the inversion of the matrix **M** (eq. 2), while the expression for the $P^{\rm w}_{\rm up}$ wavefield is obtained by including eqs (15) and (16) in eq. (14). This acoustic decomposition involves the combination of the U_h and U_z components only:

$$P^{\rm w}_{\rm down} = \frac{1}{2\alpha_{\rm w} q_{\rm w}} U_z + \frac{1}{2} U_h, \tag{19}$$

$$P^{\rm w}_{\rm up} = \frac{1}{2\alpha_{\rm w} q_{\rm w}} U_z - \frac{1}{2} U_h, \tag{20}$$

where $q_{\rm w}$ is the vertical slowness in the water layer. This decomposition can thus be performed without any *a priori* knowledge about the ocean-bottom elastic properties. The effect of the acoustic decomposition using eqs (19) and (20) is schematically illustrated in Fig. 6. Here we can note that except for the first break, the $P^{\rm w}_{\rm down}$ wavefield is simply a delayed version of $P^{\rm w}_{\rm up}$, where the time delay is the two way traveltime of the water column $Z_{\rm w}$:

$$P^{\rm w}_{\rm down} = -Z_{\rm w} P^{\rm w}_{\rm up}. \tag{21}$$

This is an interesting property that can be useful for the U_z sensor calibration (Soubaras, 1996). As for the elastic procedure, this first step does not necessary reduce the amount of water multiples in $P^{\rm w}_{\rm up}$ (compared to U_z). The amplitude of the first-order multiple (relative to a given primary) is equal to $1 - 2r$ on U_z, whereas it is equal to $2r$ on $P^{\rm w}_{\rm up}$. As a consequence, the amount of multiple energy is reduced only if $r < 0.25$ (i.e. $2r < 1 - 2r$). In the specific case of an ocean-bottom reflectivity of 0.5, the first-order multiples on $P^{w}_{\rm up}$ have the same amplitude as the associated primaries.

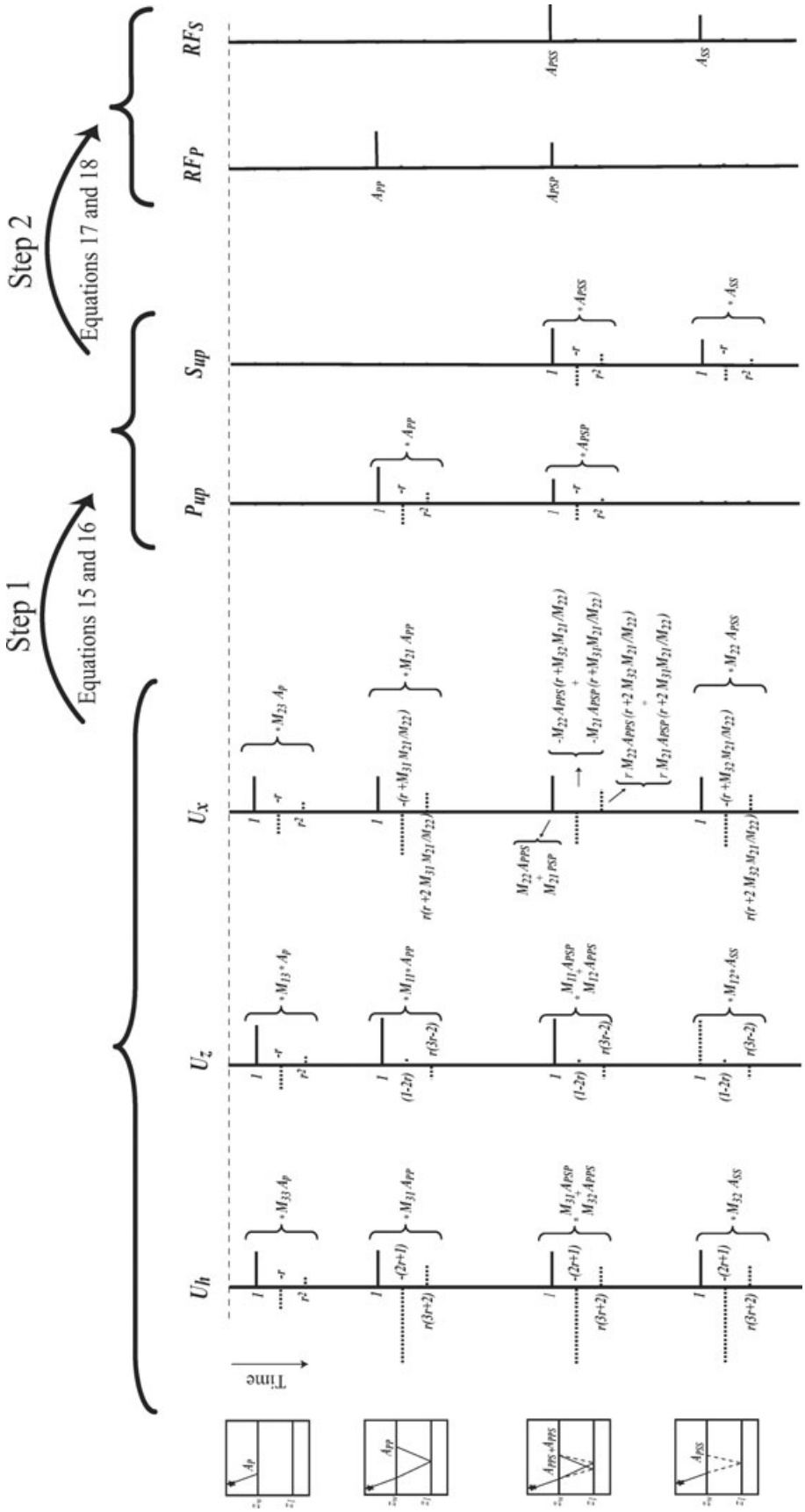

Figure 5. Overview of the RF elastic decomposition scheme in the τ–p domain. Step 1 is the *PP*–PS separation stage. Step 2 is the multiple removal stage. The final RF_P and RF_S traces contain only primary events emerging as *P* and *S* waves, respectively. The M_{ij} coefficients are those given in eqs (3)–(11).

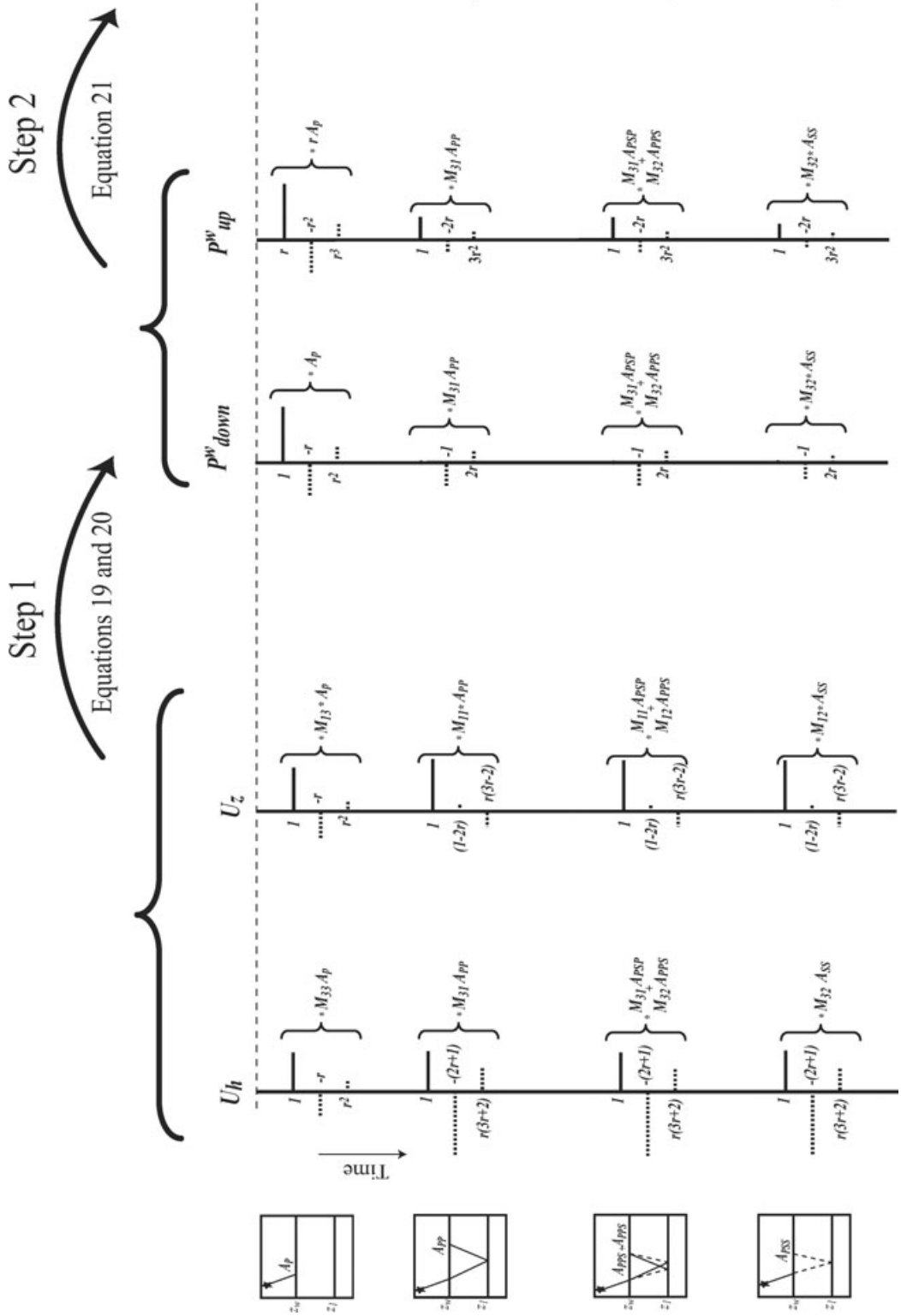

Figure 6. Overview of the acoustic decomposition scheme in the $\tau - p$ domain. Step 1 is the upgoing–dowgoing P wave separation stage. Step 2 is the first-order multiple removal stage. The M_{ij} coefficients are those given in eqs (3)–(11).

Therefore, even after decomposition using eq. (20), the multiples in $P^w_{\rm up}$ still cause problem. Soudani *et al.* (2005), as an extention of Soubaras (1996), propose a combination of the two previously estimated acoustic wavefields in the τ–p domain to eliminate the first-order of multiples:

$$RF^w_P = P^w_{\rm up} - 2r\,P^w_{\rm down}. \tag{22}$$

The effect of the subtraction is also illustrated in Fig. 6.

Compared with the elastic decomposition (RF_P, see Fig. 5), the acoustic RF^w_P is more complex because it still contains a portion of the first break and associated multiples ($Src_{\rm eff}$), as well as the second (and more) order of multiples. This demonstrates the advantage of the elastic decomposition procedure. Note, however, that the power of the acoustic scheme lies in the fact that the knowledge of the seafloor elastic properties is not required (the reflectivity r can be obtained by comparing the $P^w_{\rm up}$ and $P^w_{\rm down}$ wavefields; Soudani *et al.* 2006). Note also that Amundsen *et al.* (2001) have described in detail a water multiple removal technique, based on the use of the acoustic upgoing–downgoing wavefields, that is valid for any order, but which is computationally more expensive.

4 SYNTHETIC DATA

The effect of the decomposition schemes is now demonstrated on synthetic data computed for a simple horizontally layered medium.

Table 1. Model parameters used for the generation of synthetic data shown in Fig. 8.

depth (m)	α (km s^{-1})	β (km s^{-1})	ρ (g cm^{-3})
0–500	1.5	0	1.0
500–1000	2.1	0.6	2.0
1000–2000	2.5	1.7	2.2
2000– ∞	3.0	1.9	2.5

The model parameters are given in Table 1. The hydrophone and geophones components seismograms as a function of offset and time are displayed in Fig. 7. The source signal is a Ricker wavelet with dominant frequency of 37 Hz. The water column height $z_{\rm w}$ is 500 m. It is assumed that the geophones are located just below the seafloor whereas the hydrophone is located just above it. The offsets range from 6.25 m to 4.0 km, at 6.25 m intervals, which is finer than in typical surveys to avoid aliasing effects during the τ–p transformation. The data in the τ–p domain are shown in Fig. 8. These synthetic data have been intentionally designed to highlight the overlapping effects: up to $p = 0.4\,{\rm s\,km^{-1}}$, the reflection coefficient r is close to 0.5 (see Fig. 9) and the first-order multiples are extremely weak on U_z whereas they are very strong (relative to primaries) on U_h. The multiples appears clearly on the U_z gather only for large slownesses, when $p > 0.4\,{\rm s\,km^{-1}}$. To demonstrate the validity of decomposition equations, both the P–S separation stage and the multiple removal stage (i.e. peg-leg removal) are performed by using the correct and known α, β, ρ, r and z_w values.

4.1 Elastic decomposition results

Fig. 10 shows the two-step elastic decomposition results for the P waves. The $P_{\rm up}$ wavefield contains only primary P waves and associated peg-legs multiples. All upgoing S waves and all downgoing P waves (at the receiver level) have been removed from U_z. The first break as well as its multiples ($Src_{\rm eff}$) are efficiently removed. As expected with such model ($r \approx 0.5$), the amount of multiples is larger on $P_{\rm up}$ than on U_z (see dashed arrow just before 1.5 s, for example). However, as already mentioned, the decomposed data have now the ideal form to perform the multiple removal stage of eq. (17) (trace-by-trace), giving the RF_P gather free of any water multiples. As expected, RF_P contains only primary events emerging as upgoing P wave at the receiver. With our specific synthetic

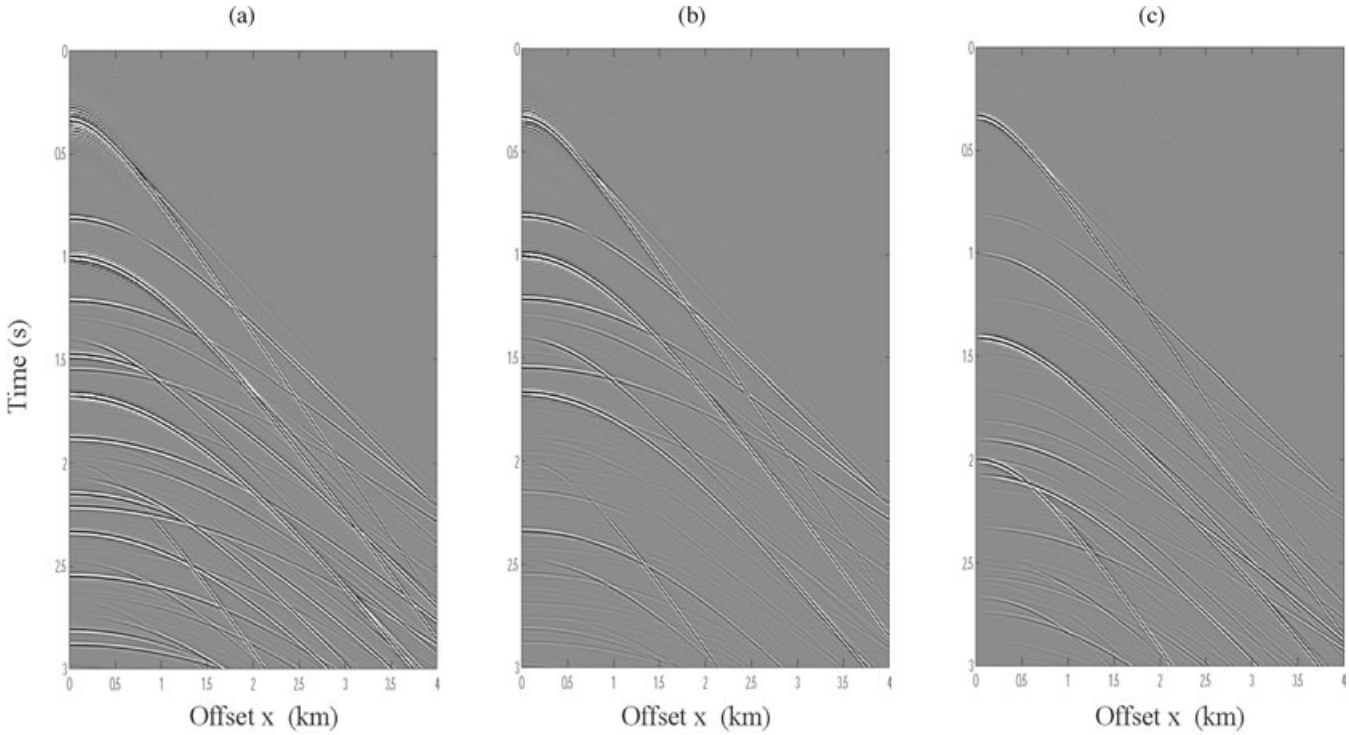

Figure 7. The synthetic OBC data in the time-offset domain. (a) U_h, (b) U_z and (c) U_x.

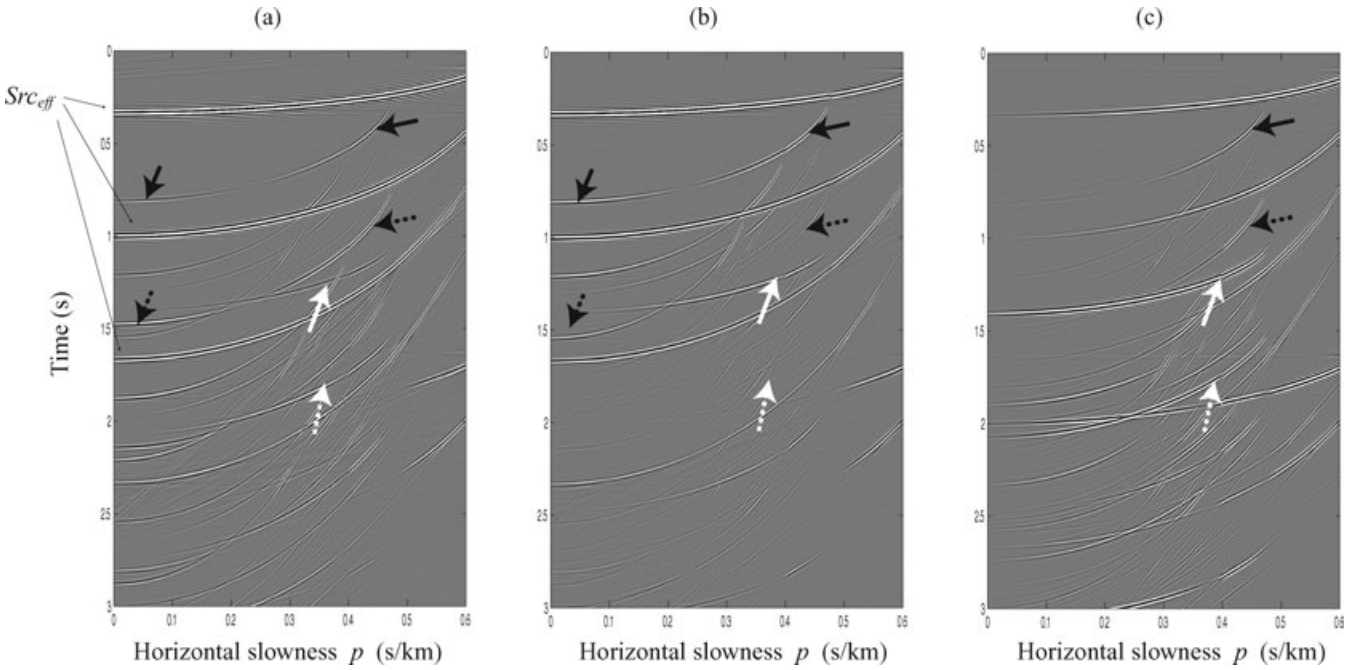

Figure 8. The synthetic OBC data in the τ–p domain. (a) U_h, (b) U_z and (c) U_x. Each component contains a mixture of all incident wave types: P waves (black arrows), S wave (white arrows) and associated (first-order) multiples (dashed arrows). Multiples clearly appear on U_h and U_x but not on U_z because of destructive effect of overlapping ghosts and peglegs.

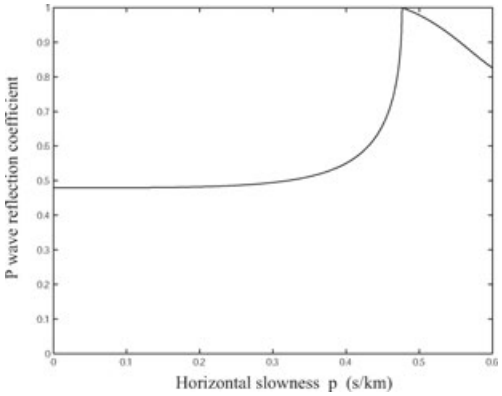

Figure 9. The seafloor P wave reflection coefficient as a function of slowness for the synthetic OBC data (with $\alpha = 2.1\,\mathrm{km\,s^{-1}}$, $\beta = 0.6\,\mathrm{km\,s^{-1}}$ and $\rho = 2.0\,\mathrm{g\,cm^{-3}}$ as seafloor elastic properties).

example, the main effect of the procedure is to remove the S wave events and the Src_{eff} arrivals, because the water multiples are already attenuated on U_z due to destructive summation of ghosts and peglegs.

Fig. 11 shows the two-step elastic decomposition results for the PS waves. The S_{up} wavefield contains only primary S-waves and associated peg-legs multiples. All P waves (both upgoing and downgoing) have been removed from U_x. Once again, the S_{up} wavefield has the ideal form to perform the multiple removal stage of eq. (18) (trace-by-trace), giving the RF_S gather free of any water multiples. As expected, RF_S contains only primary events emerging as upgoing S wave at the receiver. The arrivals with large move-out are the primary $\dot{P}\dot{P}\dot{P}\dot{S}$ waves that mostly propagate as P waves but arrive as S waves at the receiver.

4.2 Acoustic decomposition results

Fig. 12 shows the two-steps acoustic decomposition results. As shown in Fig. 1 and illustrated in Fig. 6, P^w_{up} is a resulting wavefield generated at the seafloor interface and still contains a mixture of ghost and peg-leg arrivals. As expected by the theory, with this particular data example ($r \approx 0.5$), the amount of multiple energy is larger on P^w_{up} than on the original U_z component (see dashed arrow just before 1.5 s, for example). Then the multiple removal stage of eq. (22) can be achieved giving the RF^w_P gather. Once again, as expected, the first-order multiples (dashed arrows) are correctly eliminated, but the second-order multiples as well as the Src_{eff} reverberations are still present. With our synthetic example, the acoustic scheme has a minor effect because we start from a U_z component, which is already free of (first-order) multiples.

Comparison between Figs 10 and 12 clearly demonstrates the advantage of the elastic procedure, even when dealing with the P waves only. Obviously only the elastic scheme provides the possibility of estimating the pure primary PS wavefield.

5 CONCLUSIONS

In this paper, the equations for the elastic and acoustic decomposition schemes have been derived using a simple and compatible approach. The validity of the decomposition theory has been demonstrated using a particular synthetic example. The two types of RF decomposition (i.e. elastic and acoustic) involve two steps. The first step consists of estimating the upgoing wavefields (P^w_{up} above the ocean-bottom; P_{up} and S_{up} below the ocean-bottom). The second step aims at removing the remaining multiples from these upgoing wavefields. The elastic decomposition scheme is required to process S waves and is more efficient to process P waves. We have shown that the acoustic decomposition is of limited interest, when the ocean-bottom reflection coefficient is close to 0.5. Nevertheless,

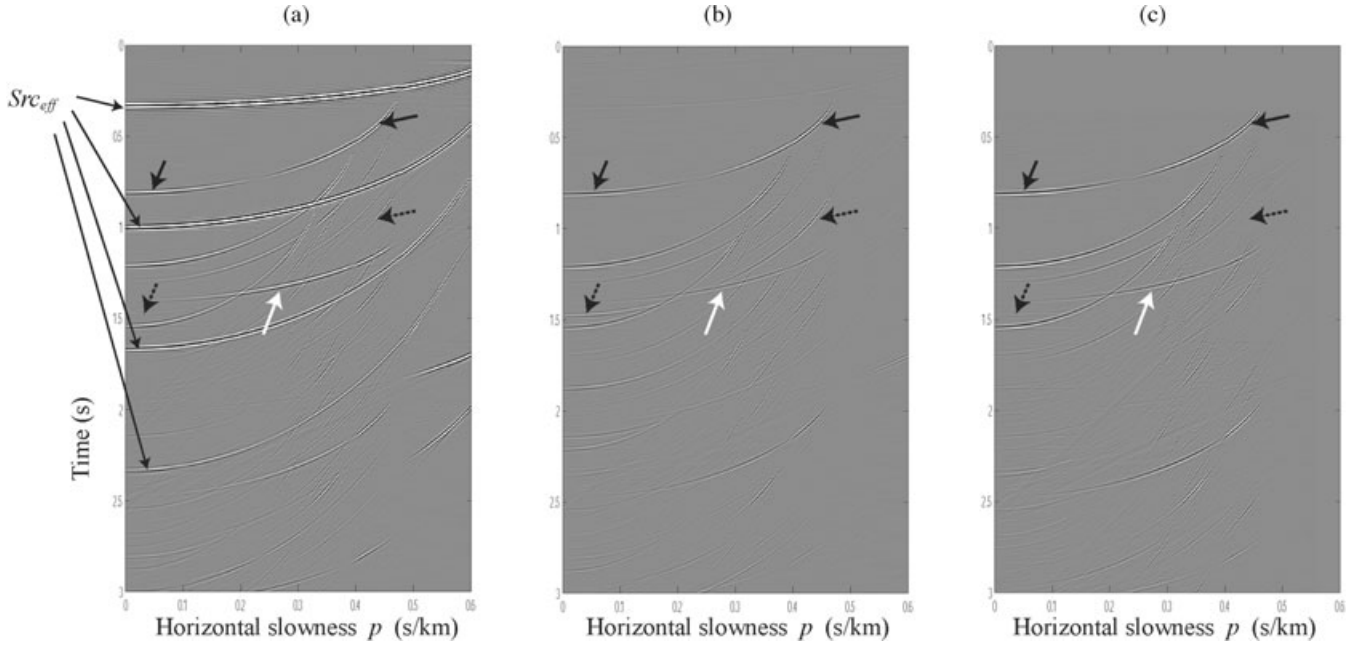

Figure 10. Elastic RF decomposition results for the P waves, in the τ–p domain: (a) U_z; (b) P_{up} and (c) RF_P. U_z is a mixture of all incident wave types: P waves (black arrows); $\grave{P}\grave{S}\acute{P} + \grave{P}\grave{P}\acute{S}$ waves (white arrows) and associated (first-order) multiples (dashed arrows). P_{up} contains only upgoing P waves, that is, primary and peg-leg arrivals. RF_P contains only primary P waves. The arrivals with low moveout are the $\grave{P}\grave{S}\acute{S}\acute{P}$ waves, propagating mostly as S waves but arriving as P wave at the receiver. For example, the white arrow on P_{up} and RF_P shows the pure $\grave{P}\grave{S}\acute{P}$ arrival.

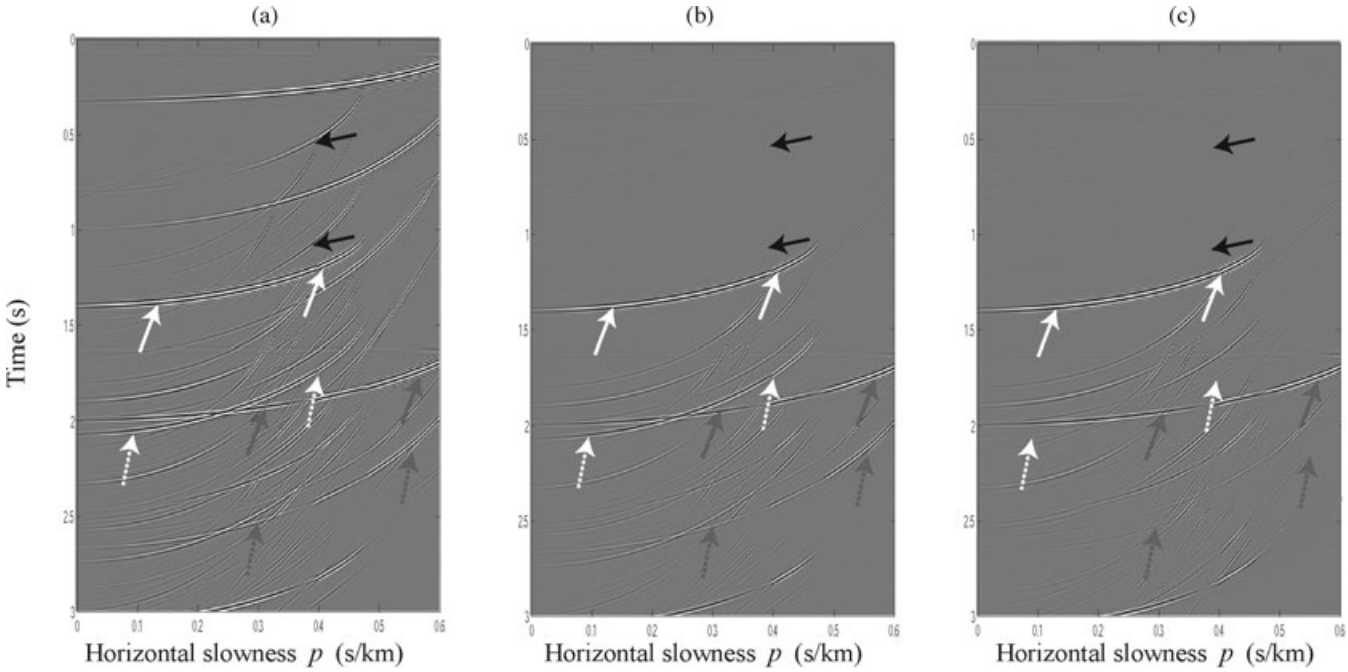

Figure 11. Elastic RF decomposition results for the S waves, in the τ–p domain: (a) U_x; (b) S_{up} and (c) RF_S. U_x is a mixture of all incident wave types: P waves (black arrows); $\grave{P}\grave{S}\acute{P} + \grave{P}\grave{P}\acute{S}$ waves (white arrows); $\grave{P}\grave{S}\acute{S}$ waves (red arrows) and associated (first-order) multiples (dashed arrows). S_{up} contains only upgoing S waves, that is, primaries and peg-legs arrivals. RF_S contains only primary S waves. The arrivals with high moveout are the $\grave{P}\grave{P}\acute{P}\acute{S}$ waves propagating mostly as P waves but arriving as S wave at the receiver.

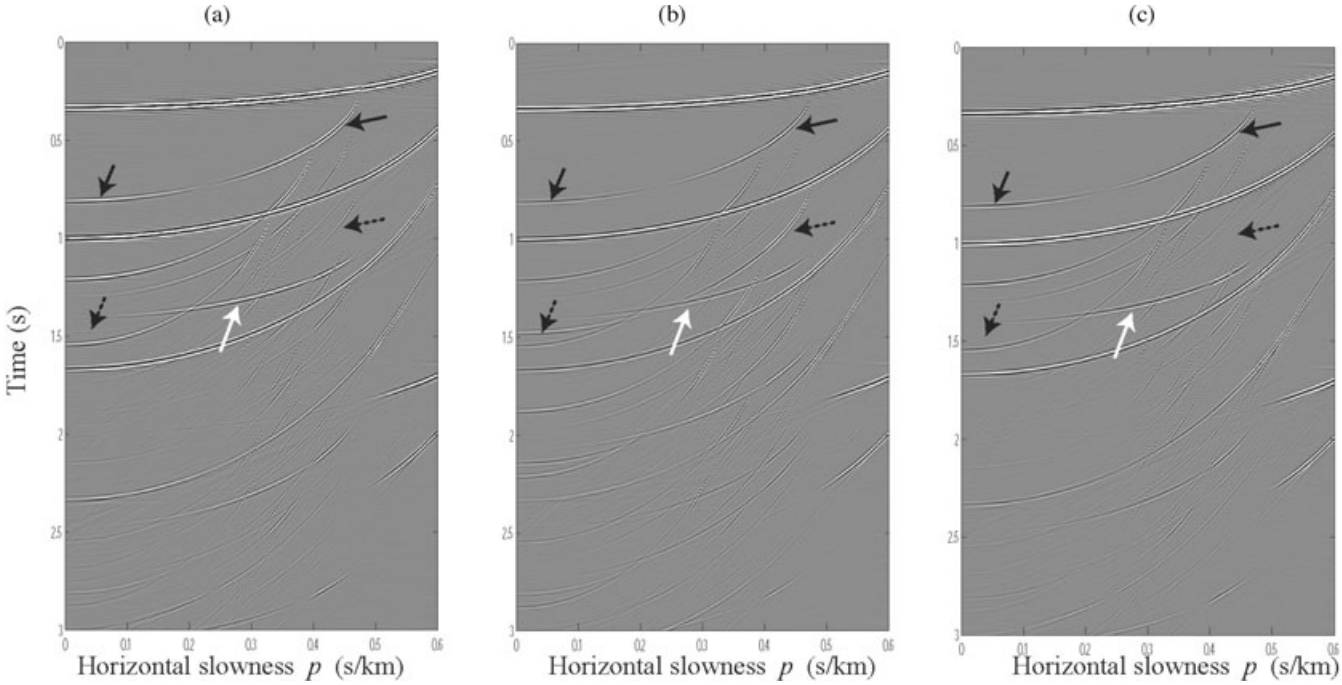

Figure 12. Acoustic RF decomposition results, in the τ–p domain: (a) U_z; (b) $P^w_{\rm up}$ and (c) RF^w_P. With these data ($r \approx 0.5$), the effect of such decomposition is minor. *P* waves (black arrows), $\grave{P}\grave{S}\acute{P} + \grave{P}\grave{P}\acute{S}$ waves (white arrows) and associated (first-order) multiples (dashed arrows).

the power of the acoustic decomposition relies on the fact that no knowledge of the ocean-bottom properties is needed, whereas the elastic decomposition requires the knowledge of the elastic properties at the ocean-bottom, in the vicinity of the receiver. For the computation of the upgoing $S_{\rm up}$ wavefield, we need the *S* wave velocity and the density values. For the computation of the upgoing $P_{\rm up}$ wavefield, we also need the *P* wave velocity.

Once the fully predictable elastic wavefields are estimated, the second stage (i.e. peg-leg removal) can be automatically processed without any additional information, using the predictive deconvolution process (when r is unknown), giving the primary *P* and *S* responses (i.e. the RF_P and RF_S gathers). The quality of the multiple removal stage naturally depends on the reliability of the first stage. The elastic properties α, β and ρ need to be accurately known to obtain the correct decomposition coefficients. Note that we assume an isotropic and horizontally layered model. Therefore, in the presence of dipping interfaces, the events may map onto slightly wrong p values in the slowness domain, and the decomposition results may degrade. If local anisotropy at the receiver level is significant, the decomposition coefficients may not be appropriate, and we may distort the estimates of amplitudes of the separated incident waves. Finally, note that when processing field data, the calibration of the sensors becomes a crucial step, often requiring the computation of frequency dependent operators to better take into account the layered feature of the sea-bed sediment formation, in addition to the different impulse responses of the recording devices. Even with the correct elastic properties, the combination of uncalibrated components will not give the expected outputs. In a following paper (Edme and Singh), we will show how to recover all the required parameters directly from the data and in an automatic way, even in challenging shallow water conditions.

ACKNOWLEDGMENTS

We would like to thank J.L. Boelle and A. Soudani for their fruitful collaboration.

REFERENCES

Amundsen, L. & Reitan, A., 1995. Decomposition of multicomponent seafloor data into upgoing and downgoing *P*- and *S*-waves, *Geophysics,* **60,** 563–572.

Amundsen, L., Ikelle, L.T. & Martin, J., 1998. Multiple attenuation and *P*/*S* splitting of OBC data: a heterogeneous sea floor, *SEG* Expanded Abstracts, **17,** 722–725.

Amundsen, L., Ikelle, L.T. & Berg, L.E., 2001. Multidimensional signature deconvolution and free-surface multiple elimination of marine multicomponent ocean-bottom seismic data, *Geophysics,* **66,** 1594–1604.

Bale, R., 1998. Plane wave deghosting hydrophone and geophone data, *SEG* Expanded abstract, **17,** 730–733.

Ball, V. & Corrigan, D., 1996. Dual sensor summation of noisy ocean-bottom data, *SEG* Expanded abstract, **15,** 28–31.

Barr, F.J. & Sanders, J.I., 1989. Attenuation of water-column multiples using the pressure and velocity detectors in a water-bottom cable, *SEG* Expanded Abstracts, **8,** 653–656.

Barr, F.J., 1997. Dual sensor OBC technology, *Leading Edge,* **16,** 45–51.

Barr, F.J., Chambers, R.E., Dragoset, W. & Paffenholz, J., 1997. A comparison of methods for combining dual-sensor ocean cable traces, *SEG* Expanded abstract, **16,** 67–70.

Chapman, C., 2004. *Fundamentals of Seismic Wave Propagation,* Cambridge University press, Cambridge.

Cho, W.H. & Spencer, T.W., 1992. Estimation of polarization and slowness in mixed wavefields, *Geophysics,* **57,** 805–814.

Dankbaar, J.W.M., 1985. Separation of *P*-waves and *S*-waves, *Geophys. Prospect.,* **33,** 970–986.

Donati, M.S. & Stewart, R.R., 1996. *P*- and *S*-wave separation at a liquid-solid interface, *J. Seism. Expl.,* **5,** 113–127.

Dragoset, W. & Barr, F.J., 1994. Ocean-bottom cable dual-sensor scalings, *SEG* Expanded abstract, **13,** 857–860.

Gal'perin, E.I., 1974. *Vertical Seismic Profiling,* Vol. 12, SEG Special Publication, SEG.

Haggerty, P.E., 1956. Method and apparatus for canceling reverberations in water layers, US Patent No. 2, pp. 757–356.

Holvik, E. & Amundsen, L., 1998. Decomposition of multicomponent sea floor data into primary *PP*, *PS*, *SP*, and *SS* wave responses, *SEG* Expanded Abstracts, **17,** 2040–2043.

Holvik, E., Osen, A., Amundsen, L. & Reitan, A., 1999. On P- and *S*-wave separation at a liquid-solid interface, *J. Seism. Expl.,* **8,** 91–100.

Kennett, B.L.N., 1983. *Seismic Wave Propagation in Stratified Media,* Cambridge university press, Cambridge.

Lines, L.R. & Treitel, S., 1984. Tutorial: a review of least-squares inversion and its application to geophysical problems, *Geophys. Prospect.,* **32,** 159–186.

Loewenthal, D., Lee, S.S. & Gardner, G.H.F., 1985. Determinist estimation of a wavelet using impedance type technique, *Geophys. Prospect.,* **33,** 956–969.

Lokshtanov, D.E., 1993. Adaptive multiple suppression in τ–p domain, *SEG Expanded Abs.,* **12,** 1086–1089.

Lokshtanov, D.E., 1995. Multiple suppression by single channel and multichannel deconvolution in the τ–p domain, *SEG Expanded Abs.,* **14,** 1482–1485.

Lokshtanov, D.E., 2000. Suppression of free-surface effects from multicomponent seafloor data, in *Proceedings of the 67th Annual EAGE meeting,* Glasgow, Expanded abstract, Session A01.

Liu, F., Sen, M.K. & Stoffa, P.L., 1999. Surface multiple attenuation for multi-component ocean-bottom seismometer data, *SEG* Expanded abstract, **17,** 1256–1259.

Muijs, R., Robertsson, J.O.A. & Holliger, K., 2004. Data-driven adaptive decomposition of multicomponent seabed seismic recordings, *Geophysic,* **69,** 1329–1337.

Muijs, R., Robertsson, J.O.A. & Holliger, K., 2007. Data-driven adaptive decomposition of multicomponent seabed seismic recordings: application to shallow-water data from the North Sea, *Geophysics,* **72,** 133–142.

Osen, A., Amundsen, L. & Reitan, A., 1999. Removal of water-layer multiples from multi-component sea-bottom data, *Geophysics,* **64,** 838–851.

Paffenholz, J. & Barr, F.J., 1995. An improved method for deriving water-bottom reflectivities for processing dual sensor ocean bottom cable data, *SEG* Expanded Abstracts, **14,** 987–990.

Robinson, E.A., 1957, Predictive decomposition of seismic traces, *Geophysics,* **22,** 767–778.

Schalkwijk, K.M., 2001. Decomposition of multicomponent ocean-bottom data into P- and S-waves, *PhD thesis*, Delft University of technology.

Schalkwijk, K.M., Wapenaar, C.P.A. & Verschuur, D.J., 2003. Adaptive decomposition of multicomponent ocean-bottom seismic data into downgoing and upgoing P- and S-waves, *Geophysics,* **68,** 1091–1102.

Soubaras, R., 1996. Ocean botton hydrophone and geophone processing, *SEG* Expanded Abstracts, **15,** 24–27.

Soubaras, R., 1998. Multiple attenuation and P-S decomposition of multicomponent ocean-bottom data, *SEG* Expanded Abstract, **17,** 1336–1339.

Soudani, M.T.A., Boelle, J.L. & Mars, J., 2005. New methodology for water layer multiple attenuation in OBC data, in *Proceedings of the 67th Meeting, European Association of Geoscientists and Engineers,* Madrid, Expanded Abstract, Session PO78.

Soudani, M.T.A., Boelle, J.L., Hugonnet, P. & Grandi A., 2006. 3D methodology for OBC pre-processing, in *Proceedings of the 68th Meeting, European Association of Geoscientists and Engineers,* Vienna, Expanded Abstract, Session BO44.

Treitel, S., 1974. The complex wiener filter, *Geophysics,* **39,** 169–173.

Wang, Y., Singh, S.C. & Barton, P.J., 2002. Separation of P and SV wavefields from multi-component seismic data in the τ–p domain, *Geophys. J. Int.,* **151,** 663–672.

Wapenaar, C.P.A., Hermann, P., Verschuur, D.J. & Berkhout, A.J, 1990. Decomposition of multicomponent seismic data into primary P- and S-wave responses, *Geophys. Prospect.,* **38,** 633–662.

White, J.E., 1965. *Seismic Waves—Radiation, Transmission and Attenuation,* McGraw-Hill Book Co, Inc, New York.

Yilmaz, O., 1987. *Seismic Data Processing,* Soc. Expl. Geophys.